

Multisensor Data Fusion for Reliable Obstacle Avoidance

Thanh Nguyen Canh¹, Truong Son Nguyen¹, Cong Hoang Quach¹, Xiem Hoang Van¹ and
Manh Duong Phung²

¹University of Engineering and Technology, Vietnam National University, Hanoi, Vietnam

²Fulbright University Vietnam, Ho Chi Minh City, Vietnam

Abstract—In this work, we propose a new approach that combines data from multiple sensors for reliable obstacle avoidance. The sensors include two depth cameras and a LiDAR arranged so that they can capture the whole 3D area in front of the robot and a 2D slide around it. To fuse the data from these sensors, we first use an external camera as a reference to combine data from two depth cameras. A projection technique is then introduced to convert the 3D point cloud data of the cameras to its 2D correspondence. An obstacle avoidance algorithm is then developed based on the dynamic window approach. A number of experiments have been conducted to evaluate our proposed approach. The results show that the robot can effectively avoid static and dynamic obstacles of different shapes and sizes in different environments.

Index Terms—Sensor fusion, obstacle avoidance, depth camera, LiDAR

I. INTRODUCTION

Obstacle avoidance is essential for the safe operation of mobile robots. This task involves the design of a sensory system for data collection and algorithms for data processing and motion planning. The sensory system may consist of single or multiple sensors depending on the working environment and application [1]. In single-sensor methods, cameras and LiDAR are widely used due to their capability to collect rich information about the environment [2]–[4]. Cameras can collect color information which allows for extracting features of the environment and obstacles. This information however is sensitive to lighting conditions causing difficulties in creating stable detection algorithms. Recent cameras can collect both color and depth information to better address the lighting issue. However, its resolution and field of view are still low. LiDAR sensors, on the other hand, can produce precise distance measurements at high frequencies. It therefore can achieve a low drift motion estimation with an acceptable computational complexity when applied to the obstacle avoidance problem [5]. However, 2D LiDARs only carries 2D information making it insufficient to cover the whole environment. 3D LiDARs are available but their price is still high for most applications. Therefore, a more relevant solution is to use multiple sensors to form a more complete picture of the environment for obstacle avoidance. In [6], [7], laser and vision sensors are used for depth estimation and obstacle avoidance. In [8], a compass sensor, a laser range finder, and an omni-directional camera are fused within a Kalman filter for location estimation and navigation. Other sensors such as Inertial Measurement

Units (IMU) [9], Ultra-Wide Band (UWB) [10], Wifi [11], and Bluetooth [12] can also be used for navigation and obstacle avoidance. One of the main issues with the use of multiple sensors is the need for calibration among the sensors. Some works address this by finding the corresponding points or edges among different sensors [13]–[15]. Some other works try to estimate the transformation matrices between the sensors [16], [17]. However, the choice of sensors and methods to calibrate them is still a challenging problem due to their differences in the information acquired, sampling frequency, accuracy, resolution, bandwidth, etc.

Apart from sensors, data processing algorithms are also important for obstacle avoidance. A number of algorithms have been developed for this task such as the vector field histogram (VFH) [18], dynamic-window approach [19], occupancy grid algorithm [20], and artificial potential field method [21]. Their effectiveness however varies depending on the sensors used and the environments in that the robot operates. Obstacle avoidance algorithms are therefore should be properly selected and optimized for the sensors and environments used.

In this paper, we propose a system that includes several sensors and a control algorithm for obstacle avoidance. The sensors include two depth cameras placed on two sides of the robot and a LiDAR placed in the middle of the cameras. The control algorithm is based on the dynamic-window approach, but uses the data fused from the sensors to calculate the input velocities. Our contributions in this study include:

- A multi-sensor obstacle avoidance system that combines both cameras and LiDAR to obtain the ability to avoid challenging objects such as tables, chairs, and moving people.
- A method to fuse data from the cameras and LiDAR to create a multi-layer map for navigation and obstacle avoidance.
- A reliable obstacle avoidance algorithm that can be implemented in an embedded computer to run in real time.

II. SENSOR DATA FUSION

This section describes our robot platform and algorithms developed for data fusion.

A. Robot platform

The robot used in this study is a differential drive mobile robot equipped with a sensory system including a 2D LiDAR

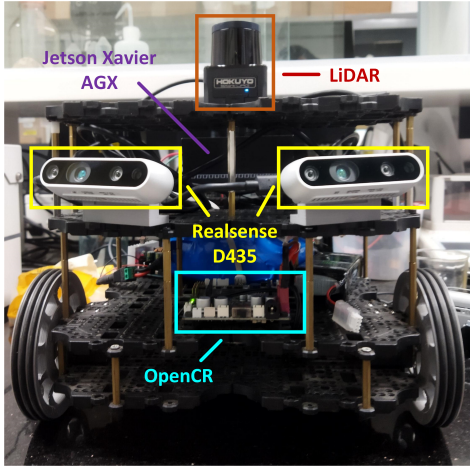


Fig. 1: The robot platform

and two depth cameras as shown Fig. 1. The LiDAR is a Hokuyo URG-20LX. The cameras are Intel Realsense D435i. The robot is driven by two Dynamixel servo motors and controlled by two onboard computers. The first computer is an OpenCR board with a built-in inertial measurement unit (IMU) for low-level control. The second one is an embedded computer called Jetson Xavier AGX used for high-level data processing and navigation. The middleware used is ROS Melodic.

For reliable navigation and obstacle avoidance, we placed the cameras at a tilted angle of 15 degrees upwards. Each camera has a horizontal field of view (FOV) of 87 degrees. The LiDAR is placed between the two cameras and has a FOV of 240 degrees. Figure 2 illustrates the overall FOV of the sensor system. With this arrangement, the LiDAR can identify objects around the robots and collect depth information about the environment for localization and mapping. The cameras, on the other hand, collect information on the whole 3D area in front of the robot and when combined with LiDAR data will provide sufficient information for obstacle avoidance. The data fusion is carried out in two stages, between the cameras and between the LiDAR and the cameras.

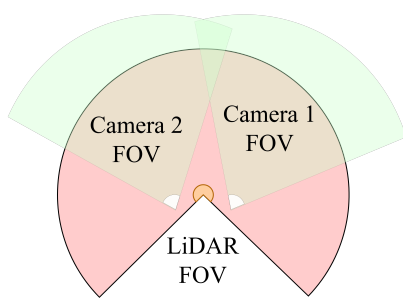


Fig. 2: Field of views of the LiDAR and cameras system

B. Depth camera data fusion

Fusing data from two cameras is the problem of finding the transformation matrix between those cameras' coordinates. Although our two cameras have a small overlap region, the information in this region is insufficient to use for calibration. Hence, we propose to use an external camera as a reference to calculate the transformation matrix, as shown in Fig. 3. We respectively estimate the transformation matrices between this external camera and the first and second cameras, and then combine those matrices to obtain the overall transformation matrix.

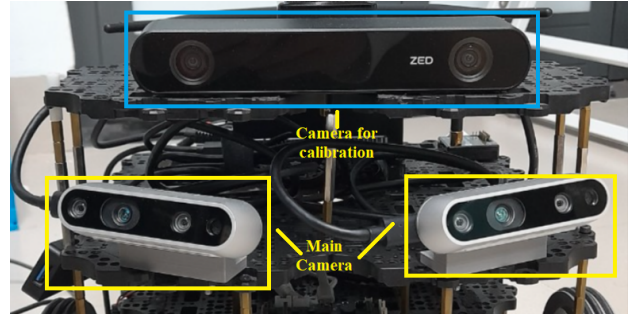


Fig. 3: Two Realsense D435 depth cameras for obstacle avoidance and one Zed2 external camera for calibration

To obtain each transformation matrix, an ArUco marker is used to convert the camera's coordinate to the coordinate attached to the ArUco marker. This marker is composed of a black border and an inner binary matrix that encodes its identifier [22]. By detecting the marker and its identifier, points on the marker can be mapped to their correspondence in the image plane. The Perspective-n-Point (PnP) problem then can be formulated and solved using methods such as EPnP [23] to find the camera pose. Denote ${}^c\mathbf{M}_o$ as the matrix representing the camera pose in the marker's coordinate frame. A point (X_c, Y_c, Z_c) in the camera's coordinate frame then can be represented by (X_o, Y_o, Z_o) in the marker's coordinate frame as follows:

$$\begin{bmatrix} X_c \\ Y_c \\ Z_c \\ 1 \end{bmatrix} = {}^c\mathbf{M}_o \begin{bmatrix} X_o \\ Y_o \\ Z_o \\ 1 \end{bmatrix} = \begin{bmatrix} {}^c\mathbf{R}_o & {}^c\mathbf{T}_o \\ 0_{3 \times 3} & 1 \end{bmatrix} \begin{bmatrix} X_o \\ Y_o \\ Z_o \\ 1 \end{bmatrix}, \quad (1)$$

where ${}^c\mathbf{R}_o$ is the rotation matrix between the marker's coordinate frame and the camera's coordinate frame, and ${}^c\mathbf{T}_o$ is the translation between the two coordinate frames.

Denote ${}^{c_1}\mathbf{M}_o$ and ${}^{c_2}\mathbf{M}_o$ as the matrices representing the poses of camera 1 and 2, respectively. The transformation between the two cameras is then computed as:

$${}^{c_2}\mathbf{M}_{c_1} = {}^{c_2}\mathbf{M}_o \times {}^o\mathbf{M}_{c_1} = {}^{c_2}\mathbf{M}_o \times ({}^{c_1}\mathbf{M}_o)^{-1} = \begin{bmatrix} {}^{c_2}\mathbf{R}_o & {}^{c_2}\mathbf{T}_o \\ 0_{3 \times 1} & 1 \end{bmatrix} \times \begin{bmatrix} {}^{c_1}\mathbf{R}_o^T & -{}^{c_1}\mathbf{R}_o^T \cdot {}^{c_1}\mathbf{T}_o \\ 0_{3 \times 3} & 1 \end{bmatrix}. \quad (2)$$

C. LiDAR and depth camera data fusion

Data fused from two cameras is a 3D point cloud as illustrated in Fig. 4a. To combine it with 2D data obtained from the LiDAR, it is necessary to convert the 3D point cloud to its 2D form. We do it by projecting the 3D point cloud to the scanning plane of the LiDAR. The projection is carried out by first calculating the coordinates of 3D points with respect to the frame attached to the LiDAR and then omitting the z component.

Since the camera is tilted upwards, we first rotate the frame attached to it to be in parallel with the LiDAR's plane. We then translate it to the origin of the LiDAR to align their two frames. Let ${}^L R_c$ and ${}^L T_c$ be respectively the rotation and translation matrices between the camera and the LiDAR. A point $P_c = (x_c, y_c, z_c)$ in the camera's frame is represented as $P_L = (x_L, y_L, z_L)$ in the LiDAR's frame as follows:

$$\begin{bmatrix} x_L \\ y_L \\ z_L \\ 1 \end{bmatrix} = \begin{bmatrix} {}^L R_c & {}^L T_c \\ 0_{3 \times 1} & 1 \end{bmatrix} \begin{bmatrix} x_c \\ y_c \\ z_c \\ 1 \end{bmatrix} \quad (3)$$

After this transformation, point P_L is represented in the LiDAR's frame with z pointing upward. Its projection to the LiDAR's plane thus can be conducted by simply setting its z coordinate to zero. Fig. 4 depicts the projected point cloud.

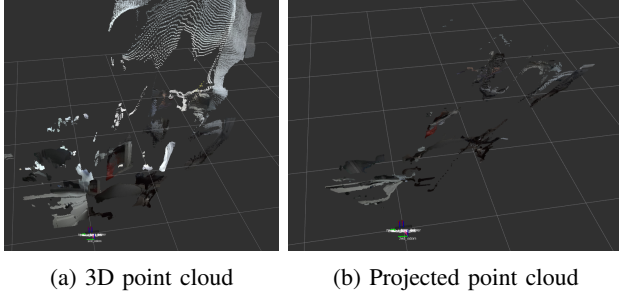


Fig. 4: Projection of a 3D point cloud to 2D

D. Multilayer fusion map

We present the fused data in a map with three layers named static, LiDAR and camera, as shown Fig. 5. The static layer represents the map of the whole working area. It is a binary grid map with value “0” for free cells and “1” for occupied cells. The LiDAR layer represents the data collected by the LiDAR during robot operation. It is a grid costmap where the value of each cell is ranged from 0 to 255 corresponding to the probability of 0% to 100% the cell being occupied. The camera layer is similar to the LiDAR layer except that it is created based on the data collected from the two cameras. During operation, the robot uses information from all three layers to reason, plan and generate control signals. For example, a cell is determined as “free” only if its value in the static map is “0” and its values in both the LiDAR and camera costmaps are less than 128. In this way, data from all sensors can be

effectively fused to provide reliable information for navigation and obstacle avoidance.

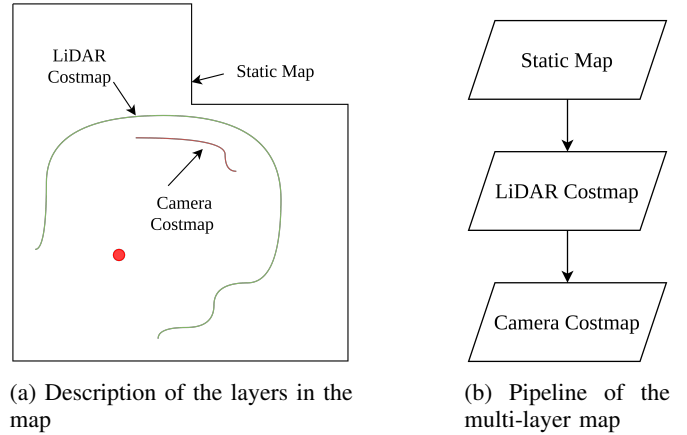


Fig. 5: Multilayer fusion map

III. OBSTACLE AVOIDANCE ALGORITHM

Based on the data fused from sensors, we developed an obstacle avoidance algorithm based on the Dynamic Window Approach method with details as follows.

A. Robot kinematics

The robot used in this work is a differential-drive robot moving on the ground plane so that its pose is determined by its position (x, y) and orientation θ . The kinematic equations of the robot are given by:

$$\begin{aligned} \dot{x} &= v \cos(\theta) \\ \dot{y} &= v \sin(\theta) \\ \dot{\theta} &= \omega \end{aligned} \quad (4)$$

where v and ω are respectively the linear and angular velocities of the robot. Since the robot is controlled by an embedded computer, it is necessary to discretize the kinematic equations. Let Δt be the sampling time and (x_t, y_t, θ_t) be the robot's pose at time step t . The discrete kinematic equations are then given by:

$$\begin{aligned} x_{t+1} &= x_t + v_t \Delta t \cos(\theta_t) \\ y_{t+1} &= y_t + v_t \Delta t \sin(\theta_t) \\ \theta_{t+1} &= \theta_t + \omega_t \Delta t \end{aligned} \quad (5)$$

In addition, ranges of the velocities are limited to:

$$V_m = \{(v, \omega) | v \in [v_{min}, v_{max}], \omega \in [\omega_{min}, \omega_{max}]\}, \quad (6)$$

where v_{max} and v_{min} are the maximum and minimum linear velocities, and ω_{max} and ω_{min} are the maximum and minimum angular velocities, respectively. Their linear and angular acceleration and deceleration are limited to $\dot{v}_a, \dot{\omega}_a$ and $\dot{v}_b, \dot{\omega}_b$, respectively.

B. Dynamic window approach

The obstacle avoidance algorithm used in this work is developed based on the dynamic window approach (DWA) [19]. This algorithm aims to find a pair of linear and angular velocity values that describe the best trajectory that the robot can achieve within its next time step. Those values are obtained via two main steps:

- 1) Determining feasible velocities based on constraints on acceleration/deceleration and obstacle avoidance.
- 2) Choosing the velocities that maximize an objective function.

In particular, the velocities that the robot can reach within its next time interval are constrained by its acceleration and deceleration limits, i.e.,

$$V_d = \left\{ (v, \omega) \mid \begin{array}{l} v \in [v_c - \dot{v}_b \Delta t, v_c + \dot{v}_a \Delta t], \\ \omega \in [\omega_c - \dot{\omega}_b \Delta t, \omega_c + \dot{\omega}_a \Delta t] \end{array} \right\} \quad (7)$$

where v_c and ω_c are respectively the present linear and angular velocities of the robot. Besides, the velocities also need to ensure that the robot does not reach its closest obstacle. Let $dis(v, \omega)$ be the distance from the robot to its closest obstacle on the trajectory generated by (v, ω) . The velocities that avoid collision are:

$$V_a = \left\{ (v, \omega) \mid \begin{array}{l} v \leq \sqrt{2 \cdot dis(v, \omega) \cdot \dot{v}_b}, \\ \omega \leq \sqrt{2 \cdot dis(v, \omega) \cdot \dot{\omega}_b} \end{array} \right\} \quad (8)$$

From (6), (7), and (8), we can limit the range of velocities to

$$V = V_m \cap V_d \cap V_a \quad (9)$$

In the second step, specific values of (v, ω) are determined from V so that they maximize the following objective function [19]:

$$G(v, \omega) = \alpha \cdot heading(v, \omega) + \beta \cdot dist(v, \omega) + \gamma \cdot vel(v, \omega), \quad (10)$$

where α, β, γ are positive weight coefficients. Function $heading(v, \omega)$ is defined as:

$$heading(v, \omega) = 1 - \frac{\theta}{\pi}, \quad (11)$$

where θ represents the angle between the robot's heading direction and the target. This function thus measures the angle deviation between the end direction of the robot's trajectory and the target. It is maximal if the robot moves directly towards the target.

Function $dist(v, \omega)$ represents the distance from the trajectory to the closest obstacle. Let d_o be the distance to the closest obstacle on the trajectory and r_e be the obstacles' expanded radius. We have

$$dist(v, \omega) = \begin{cases} \frac{1}{r} d_o & \text{if } d_o < r \\ 1 & \text{otherwise} \end{cases} \quad (12)$$

Function $vel(v, \omega)$ simply represents the linear velocity of the robot which is preferably to be fast. It is defined as:

$$vel(v, \omega) = \frac{v}{v_{max}} \quad (13)$$

By solving (10), the velocities (v, ω) that maximize $G(v, \omega)$ are the optimal velocities being applied to the robot.

IV. RESULTS

To evaluate the performance of the proposed approach, we have conducted a number of experiments with details as follows.

A. Experimental setup

Experiments have been conducted in two environments including a small corridor with the size of $50m \times 4m$ and a large room with the size of $15m \times 10m$ as shown in Fig. 6.

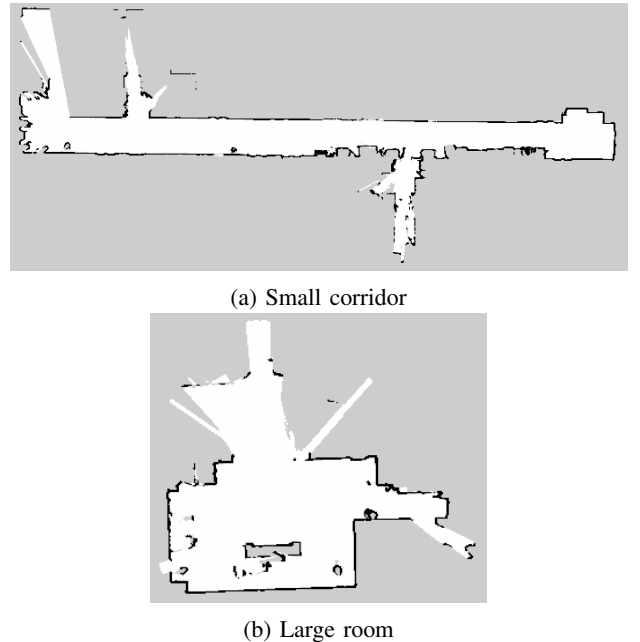


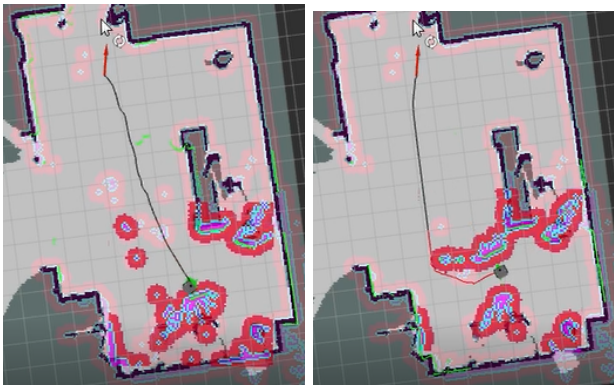
Fig. 6: Two indoor environments used in experiments

In experiments, the robot starts from its initial position A to go to its goal B. For the corridor environment, two cases with an AB distance of 10 m and 15 m are evaluated. For the room environment, two cases with the AB distance of 5 m and 10 m have been experimented. During experiments, the Cartographer SLAM algorithm was used to build maps of the environments and localize the robot. A Marvel Mind indoor locator is used to accurately estimate the robot's position, which is then used as the ground truth for comparison.

B. Experimental results

Figure 7 shows experimental results for the room environment where the black lines represent the static map, the green areas represent the LiDAR costmap, and the red areas represent obstacles. It can be seen that, without obstacles, the robot moves straight toward the goal (Fig. 7a). When obstacles appear, the robot changes its trajectory to avoid them and then navigates to the goal as shown in Fig. 7b.

To further evaluate the effectiveness of the fusion map, we test the algorithm with chair obstacles as shown in Fig. 8a. These are challenging obstacles for the LiDAR since it can only scan the legs of the chair which often leads to wrong

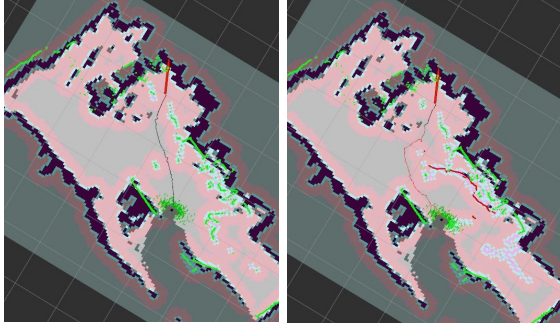


(a) The robot's trajectory when
there are no obstacles (b) The robot's trajectory when
there are obstacles

Fig. 7: Robot trajectories in the room environment



(a) Real world



(b) Obstacle avoidance path using only the LiDAR sensor
(c) Obstacle avoidance path using sensor fusion

Fig. 8: Avoiding chair obstacles in the room environment

reasoning as shown in Fig. 8b. However, when combined with the camera costmap, the robot can properly detect the obstacles to avoid and navigate to the goal as shown in Fig.8c.

For the corridor environment, experiments are also conducted with different types of obstacles including box and chair objects as shown in Fig.9a and Fig.12a. The results show that the robot can successfully detect those obstacles and avoid them as shown in Fig.9b and Fig.12b. These results can be further confirmed via positioning errors as shown in Fig.10 and Fig.11. It can be seen that the average positioning error in all scenarios is around 5 cm which is sufficient for robot operation.



(a) Real world (b) Obstacle avoidance path

Fig. 9: Avoiding chair obstacles in the corridor environment

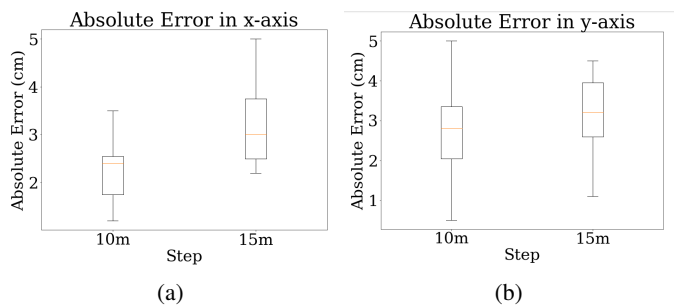


Fig. 10: Positioning errors during navigation in the corridor environment

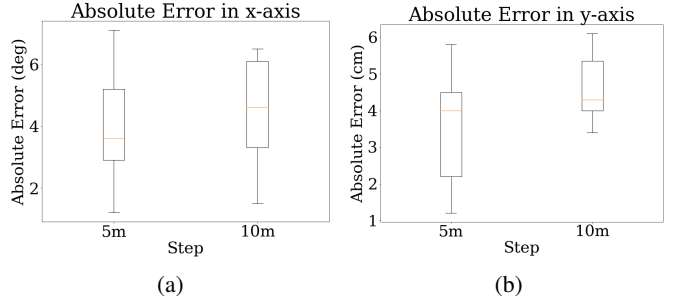


Fig. 11: Positioning errors during navigation in the room environment

Finally, we evaluate our algorithm in a dynamic environment with a person moving in the corridor as shown in (Fig. 13a). Figure 13b shows the robot's trajectory when the person is not moving. When he moves, the robot constantly adjusts its trajectory to avoid him as shown in (Fig 13c).

V. CONCLUSION

In this paper, we have proposed an approach for reliable obstacle avoidance using the data fused from multiple sensors including depth cameras and LiDAR. To fuse the data, we have introduced a calibration method based on an external camera and a projection technique to convert the 3D data to its 2D correspondence. We have also developed an obstacle

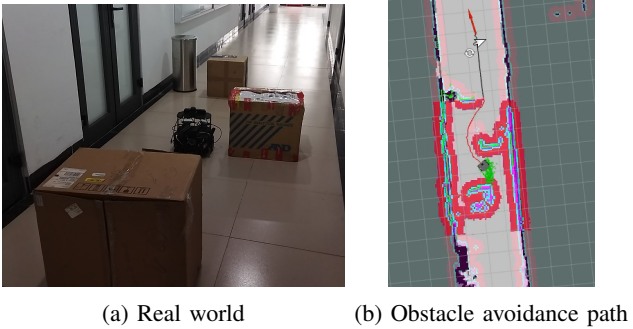


Fig. 12: Trajectory of the robot before and after fusion map during navigation in a multi-obstacle environment in a static environment

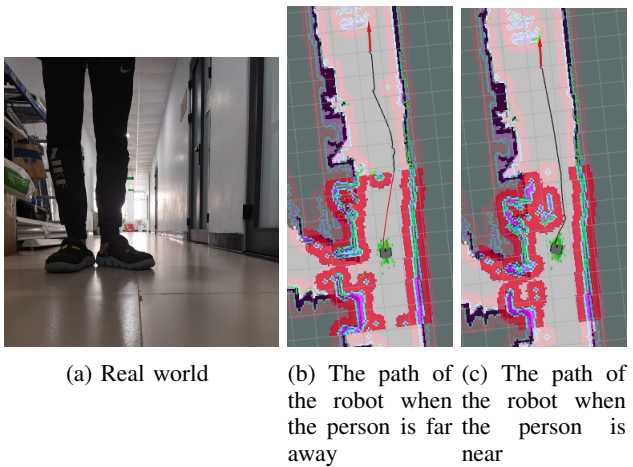


Fig. 13: Avoiding dynamic obstacles

avoidance algorithm based on the fused data and DWA. The experimental results show that our algorithm can navigate the robot to avoid different types of static and dynamic obstacles in different environments. The fused data also enhances the positioning accuracy allowing the robot to be applicable in various applications.

REFERENCES

- [1] C. Cadena, L. Carlone, H. Carrillo, Y. Latif, D. Scaramuzza, J. Neira, I. Reid, and J. J. Leonard, "Past, present, and future of simultaneous localization and mapping: Toward the robust-perception age," *IEEE Transactions on Robotics*, vol. 32, no. 6, pp. 1309–1332, 2016.
- [2] Davison, "Real-time simultaneous localisation and mapping with a single camera," in *Proceedings Ninth IEEE International Conference on Computer Vision*, 2003, pp. 1403–1410 vol.2.
- [3] C. H. Quach, V. L. Tran, D. H. Nguyen, V. T. Nguyen, M. T. Pham, and M. D. Phung, "Real-time lane marker detection using template matching with RGB-D camera," in *2018 2nd International Conference on Recent Advances in Signal Processing, Telecommunications and Computing (SigTelCom)*, 2018, pp. 152–157.
- [4] M. D. Phung, C. H. Quach, T. H. Dinh, and Q. Ha, "Enhanced discrete particle swarm optimization path planning for UAV vision-based surface inspection," *Automation in Construction*, vol. 81, pp. 25–33, 2017.
- [5] C. Debeunne and D. Vivet, "A review of visual-lidar fusion based simultaneous localization and mapping," *Sensors*, vol. 20, no. 7, 2020. [Online]. Available: <https://www.mdpi.com/1424-8220/20/7/2068>
- [6] S. Kumar, D. Gupta, and S. Yadav, "Sensor fusion of laser and stereo vision camera for depth estimation and obstacle avoidance," *International Journal of Computer Applications*, vol. 1, no. 26, pp. 22–27, 2010.
- [7] Q. Baig, O. Aycard, T. D. Vu, and T. Fraichard, "Fusion between laser and stereo vision data for moving objects tracking in intersection like scenario," in *2011 IEEE Intelligent Vehicles Symposium (IV)*, 2011, pp. 362–367.
- [8] T. T. Hoang, P. M. Duong, N. T. T. Van, D. A. Viet, and T. Q. Vinh, "Multi-sensor perceptual system for mobile robot and sensor fusion-based localization," in *2012 International Conference on Control, Automation and Information Sciences (ICCAIS)*, 2012, pp. 259–264.
- [9] G. Huang, "Visual-inertial navigation: A concise review," in *2019 International Conference on Robotics and Automation (ICRA)*, 2019, pp. 9572–9582.
- [10] L. Liu, Z. Liu, and B. E. Barrowes, "Through-wall bio-radiolocation with uwb impulse radar: Observation, simulation and signal extraction," *IEEE Journal of Selected Topics in Applied Earth Observations and Remote Sensing*, vol. 4, no. 4, pp. 791–798, 2011.
- [11] S. He and S.-H. G. Chan, "Wi-fi fingerprint-based indoor positioning: Recent advances and comparisons," *IEEE Communications Surveys & Tutorials*, vol. 18, no. 1, pp. 466–490, 2016.
- [12] R. Faragher and R. Harle, "Location fingerprinting with bluetooth low energy beacons," *IEEE Journal on Selected Areas in Communications*, vol. 33, no. 11, pp. 2418–2428, 2015.
- [13] X. Gong, Y. Lin, and J. Liu, "Extrinsic calibration of a 3d lidar and a camera using a trihedron," *Optics and Lasers in Engineering*, vol. 51, no. 4, pp. 394–401, 2013. [Online]. Available: <https://www.sciencedirect.com/science/article/pii/S0143816612003351>
- [14] Y. Park, S. Yun, C. S. Won, K. Cho, K. Um, and S. Sim, "Calibration between color camera and 3d lidar instruments with a polygonal planar board," *Sensors*, vol. 14, no. 3, pp. 5333–5353, 2014. [Online]. Available: <https://www.mdpi.com/1424-8220/14/3/5333>
- [15] A.-I. García-Moreno, J.-J. González-Barbosa, F.-J. Ornelas-Rodríguez, J. B. Hurtado-Ramos, and M.-N. Primo-Fuentes, "Lidar and panoramic camera extrinsic calibration approach using a pattern plane," in *Mexican Conference on Pattern Recognition*, 2013, pp. 104–113.
- [16] F. Vasconcelos, J. P. Barreto, and U. Nunes, "A minimal solution for the extrinsic calibration of a camera and a laser-rangefinder," *IEEE Transactions on Pattern Analysis and Machine Intelligence*, vol. 34, no. 11, pp. 2097–2107, 2012.
- [17] J. Li, X. He, and J. Li, "2d lidar and camera fusion in 3d modeling of indoor environment," in *2015 National Aerospace and Electronics Conference (NAECON)*, 2015, pp. 379–383.
- [18] J. Borenstein and Y. Koren, "The vector field histogram-fast obstacle avoidance for mobile robots," *IEEE Transactions on Robotics and Automation*, vol. 7, no. 3, pp. 278–288, 1991.
- [19] D. Fox, W. Burgard, and S. Thrun, "The dynamic window approach to collision avoidance," *Robotics and Automation Magazine, IEEE*, vol. 4, pp. 23 – 33, 04 1997.
- [20] A. Elfes, "Using occupancy grids for mobile robot perception and navigation," *Computer*, vol. 22, no. 6, pp. 46–57, 1989.
- [21] Y. Wang and G. Chirikjian, "A new potential field method for robot path planning," in *Proceedings 2000 ICRA. Millennium Conference. IEEE International Conference on Robotics and Automation. Symposia Proceedings (Cat. No.00CH37065)*, vol. 2, 2000, pp. 977–982 vol.2.
- [22] S. Garrido-Jurado, R. Muñoz-Salinas, F. Madrid-Cuevas, and M. Marín-Jiménez, "Automatic generation and detection of highly reliable fiducial markers under occlusion," *Pattern Recognition*, vol. 47, no. 6, pp. 2280–2292, 2014.
- [23] V. Lepetit, F. Moreno-Noguer, and P. Fua, "Epnp: An accurate o (n) solution to the pnp problem," *International journal of computer vision*, vol. 81, no. 2, pp. 155–166, 2009.